Assessment of Strategies for Interpolating POD Based Reduced Order Model and Application to Aeroelasticity

Fabio Vetrano[1,3]
Christophe Le Garrec[1]
Guy D.Mortchelewicz[2]
Roger Ohayon[3]

(Received: Jul. 19, 2011. Revised: Jan. 1, 2012. Accepted: Mar. 14, 2012)

Abstract
The Proper Orthogonal Decomposition (POD) technique has been widely applied to Computational Fluid Dynamics (CFD) formulation to obtain reduced-order model for unsteady aerodynamic applications. However, it should be noted that the robustness and accuracy of these reduced-order models are strictly related to the reference parameters from which POD modes have been derived. Any variation of these parameters (Mach number, angle of attack...etc) requires a new computation of the ROM which devalues the effectiveness of the POD method in an industrial application. The objective of this paper is to analyse different ROM adaptation schemes, critically describing the advantages and drawbacks of the different approaches and their application in fluid-structure interactions problems. After a general presentation of the application of the POD method to linearized Euler equations, the mathematical formulation of the interpolation schemes is presented. First a simple test on a 2D wing section is performed in transonic behaviour and then the performances of the different interpolation strategies is tested on an industrial test case.

1. Introduction

During the last two decades the evolution of computing capabilities has made possible the use of Computational Fluid Dynamics for industrial processes. An accurate model is essential to study and develop new civil transportation aircraft. To build a high fidelity aeroelastic model in the transonic regime for load calculations and aeroelastic application (flutter, gust response, etc) the use of CFD has become a superior choice over the Doublet Lattice Method or methods derived from piston theory. However, many engineering and industrial problems involving fluid-structure interaction solved by CFD required, and still required, a very large number of degrees of freedom, which may be millions, and also a large number of simulation parameters are involved in the computing process. Thus, due to the computational cost, the potential of the CFD code is currently limited to the analysis of a few configurations. For this reason, the DLM approach and correction techniques are today widely use in industrial processes. Although the computational cost of this approach is minimal and its robustness has been proved over the past years, the DLM method cannot cover every physical phenomenon which can instead be evaluated by a CFD calculation. For this purpose, several reduced-order modelling techniques have been developed in this domain. The objective of these techniques is to build a simple fluid dynamics model with a significant reduction of the degrees of freedom representative of the high fidelity model. The Karhunen-Love decomposition, also known as Proper Orthogonal Decomposition is a powerful method for computing an optimal linear base in terms of energy to represent a sample set of data and construct a reduced-order model. Unfortunately, the robustness and

[1] Airbus Operation S.A.S.
316, Route de Bayonne, 31060 Toulouse, France
[2] ONERA
29, Avenue de la Division Leclerc, 92320 Chatillon, France
[3] CNAM
2, Rue Conte, 75003 Paris, France

doi:10.3293/asdj.2011.13

accuracy of these ROMs are strictly related to the reference parameters from which POD modes have been derived. Thus, any variations in these parameters require a new computation of the POD base that is computationally expensive. For this reason, the effectiveness of the POD method in industrial applications is devalued. Since the first use of the POD/ROM technique, many efforts have been made to widen the applicability region of the ROM models and several extensions of the standard calculation method are proposed [8], [1], [5], [4], [10], [9], [6], [7], [3], [2]. At least five methods have been considered in the unsteady aerodynamic domain in the context of the POD method: The direct interpolation method [6], [16], the global POD or GPOD method [13], the subspace angle interpolation method [8], [10], [9], the sensitivity analysis method [1], [3], [2] and the Grassmann interpolation method [8], [5], [4]. The basic idea behind the direct interpolation approach is to couple the POD approach with a cubic spline interpolation procedure in order to develop fast, low-order models that accurately capture the variation in parameters, such free stream Mach number or angle of attack. The ROM vectors are orthogonal but the interpolation between orthogonal vectors is not guaranteed to construct a new set of orthogonal vectors [10]. The aim of the GPOD approach is to enrich the snapshot correlation matrix with solutions corresponding to different values of the varied parameters. A drawback of this approach is the loss of the optimal base approximation of the POD method and also failure in the transonic domain for an aeroelastic system has been shown [13]. As its name suggests, the sensitivity analysis method proposes the inclusion of parametric derivatives of the POD basis functions computed using sensitivity analysis by the finite difference method [1], [3], [2]. The subspace angle interpolation approach adapts two ROMs associated with two different parameter values to a new parameter value by linearly interpolating the subspace angles between the two precomputed basis [8], [10], [9]. The Grassmann manifold interpolation method is based on appropriately mapping the ROM data onto a tangent space to the manifold, interpolating the mapped data in this space and mapping the results back to the manifold [8], [5], [4]. This paper will present several POD/ROM adaptation techniques and evaluate their performance in different free stream conditions. In section 2 the theoretical basis for building an aeroelastic POD based Galerkin ROM from linearized Euler equations is presented. In section 3 some theoretical remarks on the three selected interpolation techniques are made. Finally in Section 4 the numerical results on NACA wing section and wind tunnel model are presented and in Section 6 some conclusions are given.

2. Theoretical Background

2.1 Linearized Euler equation

Fluid is viscous and heat-conducting and is most accurately represented by the Navier-Stokes equations. However if the Reynolds number is sufficiently high, the Prandtl number is of order unity, and separation does not occur, the viscous and heat transfer effects are confined to narrow regions near the airfoil surfaces and the wakes. Under these circumstances, the Euler equations are a good approximation of the behaviour of the flow. The unsteady Euler equations are the starting point of the linearized Euler analysis. In this paper the fluid is governed by the linearized Euler equations (LEE) in a moving mesh grid (Arbitrary Lagrangian Eulerian formulation) for steady and unsteady small disturbance inviscid flows. For the sake of brevity we will only report the principal step of the linearization process. For more details see [11]. Let $D(t)$ be a bounded fluid domain deformed over time with boundary $\Gamma(t)$. The integral form of the three-dimensional Euler equation and the geometric conservation law in a

moving Cartesian coordinate system can be written as:

$$\frac{d}{dt}\int_{D(t)} \mathbf{W} d\omega + \mathbf{F}(\mathbf{W}) = 0 \tag{1}$$

$$\frac{d}{dt}\int_{D(t)} d\omega + \int n \cdot a d\gamma = 0 \tag{2}$$

where :

$$\begin{aligned}
\mathbf{f}(\mathbf{W}) &= \left(\rho u, \rho u^2 + p, \rho uv, \rho uw(\rho e + p)u\right) \\
\mathbf{g}(\mathbf{W}) &= \left(\rho v, \rho v^2 + p, \rho uv, \rho vw(\rho e + p)v\right) \\
\mathbf{h}(\mathbf{W}) &= \left(\rho w, \rho w^2 + p, \rho vw, \rho uw(\rho e + p)w\right) \\
\mathbf{F}(\mathbf{W}) &= \int_{\Gamma(t)} \left(\mathbf{f}(\mathbf{W})n_x + \mathbf{g}(\mathbf{W})n_y + \mathbf{h}(\mathbf{W})n_z - \mathbf{a}\cdot\mathbf{n}\mathbf{W}\right) d\gamma
\end{aligned} \tag{3}$$

Equation 1 is used to obtain the discretized formulation of the Euler equations in a moving grid. Let C(t) be an elementary hexahedral cell of the computation domain with volume $\Omega(t)$. The faces of the cell are noted $\Gamma_i(t)$ (with i=1,6). The mean instantaneous field in the cell is defined by:

$$\overline{\mathbf{W}} = \frac{\int_{C(t)} \mathbf{W} d\omega}{\Omega(t)} \tag{4}$$

The discretized equations are given by:

$$\frac{d}{dt}\left(\Omega(t)\overline{\mathbf{W}}\right) + \sum_i \mathbf{F_i}(\overline{W}) = 0 \tag{5}$$

where:

$$\mathbf{F_i}(\overline{W} = \int_{\Gamma_{i(t)}} \left(\mathbf{f}(\overline{\mathbf{W}})n_x + \mathbf{g}(\overline{\mathbf{W}})n_y + \mathbf{h}(\overline{\mathbf{W}})n_z - \mathbf{a}\cdot\mathbf{n}(\overline{\mathbf{W}})\right) d\gamma \tag{6}$$

The normal to a face $\Gamma_i(t)$, dimensioned by the area of the face, is denoted:

$$\mathbf{N^i}(t) = \left(N_x^i(t), N_y^i(t), N_z^i(t)\right) \tag{7}$$

let $\overline{W}_i$ be the mean instantaneous field in the adjacent cell whose face $\Gamma_i(t)$ is common with cell $C_i(t)$. The instantaneous displacement velocity of mesh $a^i(t)$ on face $\Gamma_i(t)$ is the mean instantaneous velocity of the apexes of this face. The integral on face $\Gamma_i(t)$ is defined using Jameson's formulation:

$$\begin{aligned}
\mathbf{F_i}(\overline{\mathbf{W}}) = &\frac{\mathbf{f}(\overline{\mathbf{W}}) + \mathbf{f}(\overline{\mathbf{W_i}})}{2} N_x^i(t) + \frac{\mathbf{g}(\overline{\mathbf{W}}) + \mathbf{g}(\overline{\mathbf{W_i}})}{2} N_y^i(t) + \\
&\frac{\mathbf{h}(\overline{\mathbf{W}}) + \mathbf{h}(\overline{\mathbf{W_i}})}{2} N_z^i(t) - \mathbf{a^i}(t)\cdot\mathbf{N^i}(t)\frac{(\overline{\mathbf{W}}) + (\overline{\mathbf{W_i}})}{2}
\end{aligned} \tag{8}$$

Thus the discretized formulation of the Euler equations is given by :

$$\frac{d}{dt}\left(\Omega(t)\overline{W}\right) + \sum_i \mathbf{F_i}(\overline{\mathbf{W}}) = 0 \tag{9}$$

The geometric conservation law (Equation 2) is written:

$$\frac{d}{dt}\left(\Omega(t)\right) + \sum_i \left(\mathbf{a^i(t)}\cdot\mathbf{N^i(t)}\right) = 0 \tag{10}$$

To linearize equations 9 and 10, the mean instantaneous field $\overline{W}$ is divided into a steady mean field $\overline{W}_s$ and a fluctuation $\delta\overline{W}$:

$$\overline{W} = \overline{W}_s + \delta\overline{W} \tag{11}$$

Similarly the instantaneous position of the grid nodes is divided into a steady part and a fluctuation around a steady state:

$$M(i) = M_s + \delta M(i) \tag{12}$$

If a periodic solution with period T is sought, fluctuation $\delta M(t)$ around steady state M_s is periodic and centred:

$$\delta M(t+T) = \delta M(t) \tag{13}$$

$$\int_0^T \delta M(i) di = 0 \tag{14}$$

The assumption made is that low amplitude fluctuations $\delta M(t)$ (first order) of the grid create fluctuations $\delta\overline{W}$ of the mean field which are of the same order of magnitude. A Taylor series expansion can be performed on computation of the volume and normals. Only the first order is used:

$$\Omega(t) = \Omega_s + \delta\Omega(t) \tag{15}$$

$$N^i(t) = N_s^i + \delta N^i(t) \tag{16}$$

A Taylor series expansion around the steady solution is performed. Only the first-order terms are used to obtain the discretized formulation of the linearized Euler equations in a moving grid:

$$\begin{aligned} &\frac{d}{dt}(\Omega_s\delta\overline{W} + \delta\Omega(t)W_s) + \sum_i (\frac{1}{2}(f(\overline{W}) + f(\overline{W_{si}}))N_x^i(t) + \\ &(g(\overline{W}) + g(\overline{W_{si}}))N_y^i(t) + (h(\overline{W}) + h(\overline{W_{si}}))N_z^i(t) + \\ &\frac{1}{2}([A](W_s)\delta W + [A](W_{si})\delta W_i)N_{sx}^i + \frac{1}{2}([B](W_s)\delta W + [B](W_{si})\delta W_i)N_{sy}^i + \\ &\frac{1}{2}([C](W_s)\delta W + [C](W_{si})\delta W_i)N_{sz}^i + a^i(t)\cdot N_s^i(t)\frac{1}{2}(\overline{W} + \overline{W_i})) = 0 \end{aligned} \tag{17}$$

The above equations system can be written as:

$$[A_0(W_s)]\delta W + [A_1(W_s)]\frac{\partial \delta W}{\partial t} = [B_0(M_s)] + [B_1(\frac{\partial \delta M_s}{\partial t})] \tag{18}$$

Where $[A_0(W_s)]$, $[A_1(W_s)]$ are real matrices and $B_0(M_s)$, $B_1(\frac{\partial \delta M_s}{\partial t})$ are real vectors. Euler equations are solved on a multi-block structured mesh using the Jameson-Lerat scheme introduced in the computer code REELC developed at ONERA.

2.2 POD Galerkin Reduced-Order Model

Reduced-order modelling with POD is essentially analysis by an empirical spectral method. With spectral methods, field variables are approximated using expansions involving chosen sets of basis functions. The Galerkin equations are manipulated to obtain sets of equations for the coefficients of the expansions that can be solved to predict the behaviour of field variables in space and time. The POD is an alternative basis that is derived from a set of system observations. In short, samples, or snapshots, of system behaviour are used in a computation of appropriate sets of basis functions to represent system variables. The POD is remarkable in that the selection of basis functions is not just appropriate, but optimal, in a sense to be described further. The need to obtain samples of system behaviour to construct the POD-based ROM is both a strength and weakness of the method. One strength is that models can be efficiently tuned to capture physics in a high-fidelity model. Two noteworthy weaknesses are the need to compute samples with a high-order, high fidelity method, and the possible lack of model robustness to changes in parameters that govern system

behaviour. Generally, the pay-off in applying POD is quite high when, following an initial computation investment, a compact ROM can be constructed that can be used many times in, say, a multidisciplinary environment and which is valid over a useful range of system states [19]. In the following we will show the different steps to building an aeroelastic POD based Reduced Order Model.

2.3 Snapshots and POMs computation

The starting point of the POD based ROM procedure is calculating the small disturbance solution response of the fluid dynamic system at N different combinations of excitation and frequency. These solutions, also known as snapshots, are denoted by $U = \left\{u^1, \ldots, u^N\right\}$. The Euler equations, solved for the special case of a harmonic excitation $(M_s, t) = d(M_s)e^{i\omega t}$, lead to a search for a solution of the form $U = Ue^{i\omega t}$, where d is a prescribed structural displacement field, ω is the frequency and $i = \sqrt{-1}$ is the imaginary number. Thus the snapshots are the estimate of the complex unsteady field at the center of the j-th cell of the computational grid for a varying frequency ω. In particular, four dependent variables are stored in snapshots for each computational cell in the case of two-dimensional Euler equations and five dependent variables in the case of three-dimensional Euler equations. The POD technique is then used to find the smallest and best subspace of finite dimension $M << N$ which contains the dominant unsteady characteristics of the flow. The identified subspace $\Psi^i, i = 1, .., M$ represents the dominate ""directions"" of the full original solution. Each snapshot can be approximated by a POM (Proper Orthogonal Mode also known as POD vectors) linear combination:

$$u^n = \overline{u} + \sum_{i=1}^{N} \eta_i \Psi^i \tag{19}$$

The POD modes are obtained from the maximization problem:

$$\max_{\Psi} \langle \| \left(u(t), \frac{\Psi}{\|\Psi\|} \right) \frac{\Psi}{\|\Psi\|} \|^2 \rangle \tag{20}$$

We maximise the norm of the u projection on the right vectorial direction of Ψ on average on T, where T is a discrete or continuous ensemble. Note that in general the following equivalent formulation is preferred:

$$\max_{\Psi} \langle \frac{(u(t), \Psi)^2}{(\Psi, \Psi)} \rangle \tag{21}$$

The previous problem is equivalent to the resolution of the following eigenvalues problem

$$SV = V\lambda^2 \tag{22}$$

Where S is the real snapshot correlation matrix

$$S = RR^T \tag{23}$$

with,

$$R = (Re(U)\ Im(U)) \tag{24}$$

and each column of U contains a complex valued snapshot. V is an eigenvector. The choice of eigenvector to build the POD basis is made according to the following criteria:

- Snapshots that are not decorrelated. The modes obtained from decorrelated snapshots are the snapshots themselves and they all have the same eigenvalues;
- Elimination of the eigenvectors associated with eigenvalues that are zero or too small.

- There is little difference between partial and total energy

As shown in [15] the POMs are a simply linear rearrangement of the original snapshots:

$$\Psi^i = \sum_{n=1}^{N} a_m^i u^n \tag{25}$$

After the eigenvalues problem has been solved (Equation 22) the POMs are computed by equation 25 where

$$a_m^i = V_M \lambda_M^{-1} \tag{26}$$

2.4 Galerkin projection

After having computed the POD basis the next step, to obtain a fluid ROM, is to project the governing fluid equation on to the reduced base. If we consider a disturbance field such as:

$$U = [\Psi]\,\eta \tag{27}$$

Where η is the vector of the components of the disturbance field in the POD base. The reduced system is obtained by projecting the linearized Euler equations into the POD basis:

$$[\Psi]^H \left([A_0]\,U + [A_1]\,\frac{\partial U}{\partial t} \right) = [\Psi]^H \left([B_0]\,(d) + [B_1] \left(\frac{\partial d}{\partial t} \right) \right) \tag{28}$$

The reduced order model obtained is:

$$[a_0]\,\eta + [a_1]\,\frac{\partial \eta}{\partial t} = b_o(d) + b_1 \left(\frac{\partial d}{\partial t} \right) \tag{29}$$

Where the fluid system matrix $[a_0]$, $[a_1]$ and the coupling vector b_0, b_1 can be significantly smaller than their full-order counterparts. For more theoretical details on the Galerkin projection see [12].

2.5 Generalized Aerodynamic Forces

Once the fluid ROM has been calculated, the corresponding aerodynamic force may be determined. The displacement field d is linked to the structural modes φ by

$$d = [\varphi]\,q \tag{30}$$

Where q represents the generalized coordinates. For each structural mode φ_m, vectors $b_0(\varphi_m)$ and $b_1(\varphi_m)$ can be calculated. These vectors are stored in columns in matrix $[b_0]$ and $[b_1]$. The reduce order model is:

$$[a_0]\,\eta + [a_1]\,\frac{\partial \eta}{\partial t} = [b_0]\,q + [b_1]\,\frac{\partial q}{\partial t} \tag{31}$$

The variation of the pressure field caused by a mode of the POD basis is independent of the boundary conditions applied to the structure. This means that we can generate a vector of the GAF for each structural mode. These vectors are stored in a matrix $[F]$. The generalized aerodynamic forces are then related to the vector η by:

$$GAF = [F]\,\eta \tag{32}$$

2.6 Coupled Fluid/Structural Aeroelastic Model

In summary, the POD method outlined above leads to a reduced order basis that can be used for building an aerodynamic ROM for a given free stream Mach number and angle of attack. The corresponding aeroelastic system is obtained by coupling the equations 31, 32 and 33. Let us introduce the equation for a

coupled fluid-structure aeroelastic system. The motion of a body with respect to an equilibrium position, in the Laplace domain, is described by the equation

$$\sum_{n}^{M} M_{nm}\ddot{q}_m + \sum_{n}^{M} C_{nm}\dot{q}_m + \sum_{n}^{M} K_{nm}q_m + \frac{1}{2}\rho_\infty V_\infty^2 \sum_{n}^{M} F_{nm}\left(M_\infty V_\infty\right) q_m = 0 \tag{33}$$

with $C_{nm} := 2\xi_m\sqrt{K_{nm}M_{nm}}\delta_{nm}$ and where δ_{nm} is the Kroneker symbol, q is the generalized coordinates, K_{nm} is the stiffness matrix, M_{nm} is the mass matrix, C_{nm} is the damping matrix and F_{nm} is the aerodynamic pressure force. If we put the aeroelastic equation and the POD equation in the same equation system we obtain:

$$\begin{cases} [m]\,\ddot{q} + [c]\,\dot{q} + [k]\,q + \frac{1}{2}\rho_\infty V_\infty^2\,[f]\,q = 0 \\ [a_0]\,\eta + [a_1]\,\frac{\partial \eta}{\partial t} = [b_0]\,q + [b_1]\,\frac{\partial q}{\partial t} \\ GAF = [F]\,\eta \end{cases} \tag{34}$$

We can write the ROM aeroelastic model in the state space model like:

$$\left(\begin{bmatrix} I_d & 0 & 0 \\ 0 & [m] & 0 \\ [-b_1] & 0 & [a_1] \end{bmatrix}\right)\frac{d}{dt}\begin{pmatrix} q \\ \dot{q} \\ \eta \end{pmatrix} = \left(\begin{bmatrix} 0 & [I_d] & 0 \\ [-k] & [c] & \frac{1}{2}\rho_\infty V_\infty^2\,[F] \\ [-b_0] & 0 & [-a_0] \end{bmatrix}\right)\begin{pmatrix} q \\ \dot{q} \\ \eta \end{pmatrix} \tag{35}$$

This is a linear system, thus any stability study is reduced to finding the eigenvalues of a generalized linear system.

3. Interpolation Method Between POD Basis

The main drawback of a POD/ROM approach, such as that described in Section 1, is the lack of robustness over an entire parameter space. This is partly because the snapshots are representative only of the operating point (Mach and AoA) for which they are computed. Thus, any ROM generated by the approach outlined above cannot be expected to give a good approximation of the fluid subsystem away from the operating point [9]. For this purpose, different approaches have been developed to adapt a POD basis to address a parameter variation without recomputing the snapshots for the new parameters. The selection of the methods to interpolate between POD basis has been done in the present work, taking into account state of the art POD/ROM interpolation techniques in the aeroelastic domain.

3.1 Sensitivity Analysis Method

The objective of the sensitivity analysis method is to derive the first-order total derivatives of the POD modes Ψ_i with respect to a generic parameter α. In this study they are computed by a second-order centered finite-difference approximation:

$$\frac{D\Psi_i}{D\alpha}\left(x(\alpha_0);(\alpha_0)\right)|_{FD} = \frac{\Psi_i\left(x(\alpha_0+\Delta\alpha_0);(\alpha_0+\Delta\alpha_0)\right) - \Psi_i\left(x(\alpha_0-\Delta\alpha_0);(\alpha_0-\Delta\alpha_0)\right)}{2\Delta\alpha_0} \tag{36}$$

where α_0 is the parameter value at which the sensitivities are computed and $\Delta\alpha$ is the step in the finite-difference scheme. $\frac{D}{D\alpha}$ represents the total derivative with respect to α. The parameter increment $\Delta\alpha$ is chosen sufficiently small for the finite-difference computation to be accurate and sufficiently large for the difference between the two nearby POD vectors to be at least one order of magnitude larger than the discretization error. We treat each POD mode as a function of both space and parameter: $\Psi_i = \Psi_i(x;\alpha)$. A change of $\Delta\alpha$ in

the parameter from its baseline value α_0 is reflected in the modes through a first-order expansion in the parametric space:

$$\Psi_i(x;\alpha) = \Psi_i\left(x(\alpha_0);\alpha_0\right) + \Delta\alpha \frac{D\Psi_i}{D\alpha}\left(x(\alpha_0);\alpha_0\right) + O(\Delta\alpha^2) \tag{37}$$

Another formulation is considered by the authors in [1], [3], [2] but for the sake of brevity we will only look at the extrapolated basis formulation. It should be noted that with the sensitivity analysis method only the variation of one parameter (Mach or angle of attack) can be taken into account. In the following, finite difference approach and sensitivity analysis are used to indicate the same interpolation technique.

3.2 Subspace Angle Interpolation Method

This method uses the concepts of principal angle between two subspaces and principal vectors for a pair of subspaces [14]. The smallest angles θ_k (also known as the principal angles) between two subspaces M and N are defined by:

$$\cos\theta_k = max_{u\in M_{k-1}^{\perp}} max_{v\in N_{k-1}^{\perp}} u^H v = u_k^H v_k \tag{38}$$

The vectors $(u_1, .., .., u_k)$ and $(v_1, .., .., v_k)$ are called principal vectors of the pairs of space. The principal angle $\theta_k$can be interpreted as the set of angles providing a series of rotations that transform one of the two subspaces considered into the other one. Different methods are proposed by Bjorg for computing these angles, in this paper we have chosen the Single Value Decomposition approach proposed in [14]. Let Φ_1 and Φ_2 be two matrices storing the POD basis vectors Ψ_i built for two different values of a model parameter (Mach or AoA), and let Y, Γ and Z be the matrices obtained by the Single Value Decomposition

$$\Phi_1^T \Phi_2 = Y\Sigma Z \tag{39}$$

The cosines of the principal angle are given by:

$$\cos\theta_k = \Sigma \tag{40}$$

And the principal vectors are given by

$$\begin{aligned} U &= Y\Phi_1 \\ V &= Z\Phi_2 \end{aligned} \tag{41}$$

We can now construct a new POD basis at arbitrary parameter values α_N with $\alpha_1 < \alpha_N < \alpha_2$ by computing the principal angle by linear interpolation as follows:

$$\theta_k(\alpha_1, \alpha_N) = \left(\frac{\alpha_N - \alpha_1}{\alpha_2 - \alpha_1}\right)\theta_k\left(\alpha_1, \alpha_2\right) \tag{42}$$

Then, noting that each principal angle represents the rotation through which a basis vector of one subspace can be transformed into a basis vector of the other subspace, using simple geometry considerations we can write the new POD basis as:

$$\overline{\Psi}_k\left(\alpha_N\right) = u_k \cos\theta_k(\alpha_1, \alpha_N) + \frac{v_k - (u_k^T v_k)u_k}{\|v_k - (u_k^T v_k)u_k\|^2} \sin\theta_k(\alpha_1, \alpha_N) \tag{43}$$

It should be noted that with the Subspace angle interpolation only the variation of one parameter (Mach or angle of attack) can be take into account.

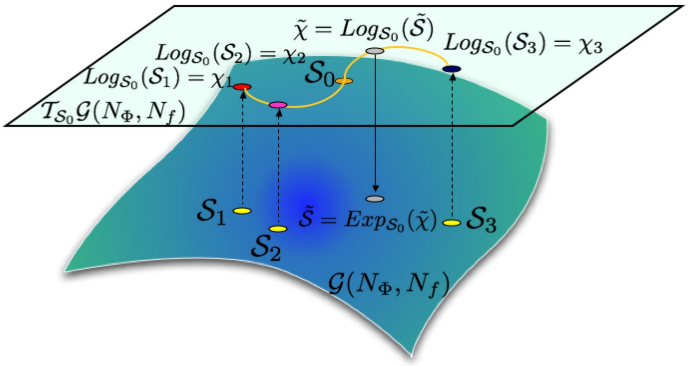

[7]

Figure 1: A graphical description of the interpolation of four subspaces in a tangent space to a Grassmann manifold (figure courtesy of Prof. C. Farhat, Stanford).

3.3 Grassmann Manifold Interpolation Method

The aim of the Grassmann manifold interpolation approach is to solve typical problems that normally concern POD interpolation techniques, such as the orthogonality property of the ROM basis after interpolation. For this reason, the interpolation is made in a flat constraint free space. For the sake of brevity in this paper we will only show the principal step of the adaptation procedure. For more theoretical detail on differential geometry see [17], [20].

Let Φ_0 and Φ_i represent different reduced-order bases pre-computed at different operating points λ_0 and λ_i corresponding to different values s_0 and s_i of a physical parameter s. The proposed procedure for adapting the available reduced-order basis to a new operating point $\overline{\lambda}$ corresponding to a value $\overline{s}$ of s that is different from both s_0 and s_i can be described in this case as follows. The first step of the Grassmann manifold interpolation method consists in the choice of the origin point S_{i_0} of the manifold as a reference and origin point for the interpolation. Each point S_i in the tangent space $T_{S_{i_0}}$, that is sufficiently close to S_{i_0}, is mapped to a matrix Γ_i representing a point χ_i of $T_{S_{i_0}}$ using the logarithm map $\log_{T_{S_{i_0}}}$. This can be written as:

$$(I - \Phi_0\Phi_0^T)\Phi_i(\Phi_0^T\Phi_i)^{-1} = U\Sigma V^T \tag{44}$$

$$\Gamma_i = U\tan^{-1}(\Sigma)V^T \tag{45}$$

Since the tangent space $T_{S_{i_0}}(\mathrm{G})$ is a flat vector space, it is possible to interpolate the Γ_i on this plane to obtain the following approximation.

$$\overline{\Gamma} = \left(\prod_{i\neq j}\frac{\overline{s} - s_j}{s_i - s_j}\right)\Gamma_i \tag{46}$$

Different interpolation schemes are proposed: in the case of one physical parameter variation (Mach or AoA) contained in each operating point, a univariate Lagrange type interpolation scheme is chosen. Otherwise, in the case of a simultaneous variation of multiple parameters (Mach and AoA), a multivariate interpolation scheme is chosen [18], [21]. The matrix $\overline{\Gamma}$ representing $\overline{\chi} \in T_{S_{i_0}}$ is mapped to a subspace $\overline{S}$ on the Grassman manifold spanned by a matrix $\overline{\Phi}$ using the exponential map $\exp_{S_{i_0}}$. This can be written as

$$\overline{\Gamma} = \overline{U}\tan^{-1}\overline{\Sigma}\,\overline{V}^T \tag{47}$$

$$\overline{\Phi} = \Phi_0\overline{V}\cos\overline{\Sigma} + \overline{U}\sin\overline{\Sigma} \tag{48}$$

The above algorithm it is graphically depicted in Figure 1 [7]. As shown above, it should be noted that the Grassmann interpolation is able to take into account the simultaneous variation of multiple parameters (Mach number or angle of attack).

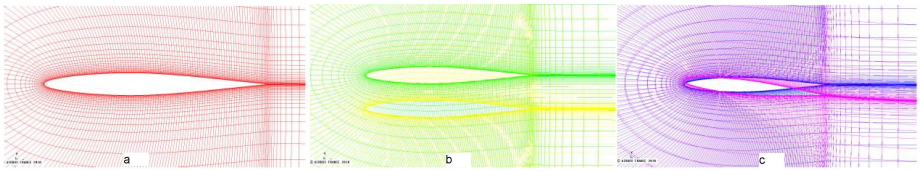

Figure 2: Computational grid for NACA 64A010 airfoil.

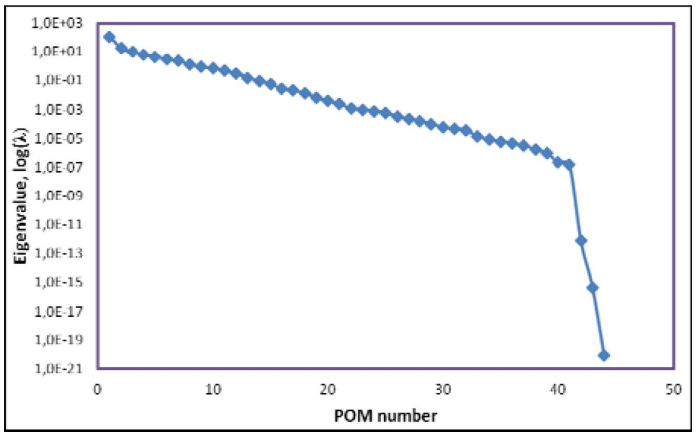

Figure 3: Eigenvalues λ distribution of the correlation matrix computed for the NACA 64A010

4. Numerical results and discussion

A critical review of the selected methods is now applied to two different aeroelastic systems, a NACA 64A010 wing section and a transonic wind tunnel model representative of an Airbus commercial aircraft.

4.1 NACA 64A010 Wing Section

The aeroelastic full order computational model consists of a CFD structured Euler C-mesh with 6888 cells, which corresponds to 27552 flow perturbation unknowns, see Figure 2(a), and two structural modes, obtained by a vertical rigid translation (Figure 2(b)) and a pitch rotation around the quarter chord (Figure 2(c)) of the aerodynamic mesh. For all simulations total pressure and total temperature are fixed respectively at 203321 Pascal and 310 Kelvin. POD basis vectors were calculated using a frequency domain method of the snapshot approach. The reduced frequency k is defined as:

$$k = \frac{\omega c}{U} \tag{49}$$

where ω is the frequency of the airfoil motion, c is the wing section chord and U is the freestream velocity. In order to compute the POD basis vectors, complex flow snapshots are evaluated at 11 evenly spaced, reduced frequencies between 0 and 0.3 for each structural mode for a total of 44 real POD vectors (2 Modes * 11 Frequencies * Real and Imaginary part of the snapshots).

Having computed the snapshots, we next use the technique described in Section 2.3 to find the POD vectors. Figure 3 shows the eigenvalues distribution of the correlation matrix. A sudden drop is seen starting at 42 vectors, meaning that the most of the energy is contained in the first 42 POD vectors.

Once the POD basis has been built for each configuration, the adaptation capabilities of the different techniques are tested in three different conditions: two low transonic cases and one high transonic case. The objective was to evaluate the influence of the delta between the POD basis chosen for the interpolation and its influence on the results. First the adaptation capability to a change in a free stream Mach number was investigated. Then the adaptation to a simultaneous change in a free stream Mach number and angle of attack was investigated. A set of three POD basis are pre-computed at low transonic free-stream Mach numbers as shown in Table 1, which also shows the new Mach

Method	M_1	M_2	M_3	M_{Int}
Angle	0.7	0.75	X	0.725
Finite Diff.	0.7	0.75	0.8	0.725
Grassmann	0.7	0.75	0.8	0.725

Table 1: Set of precomputed ROM basis

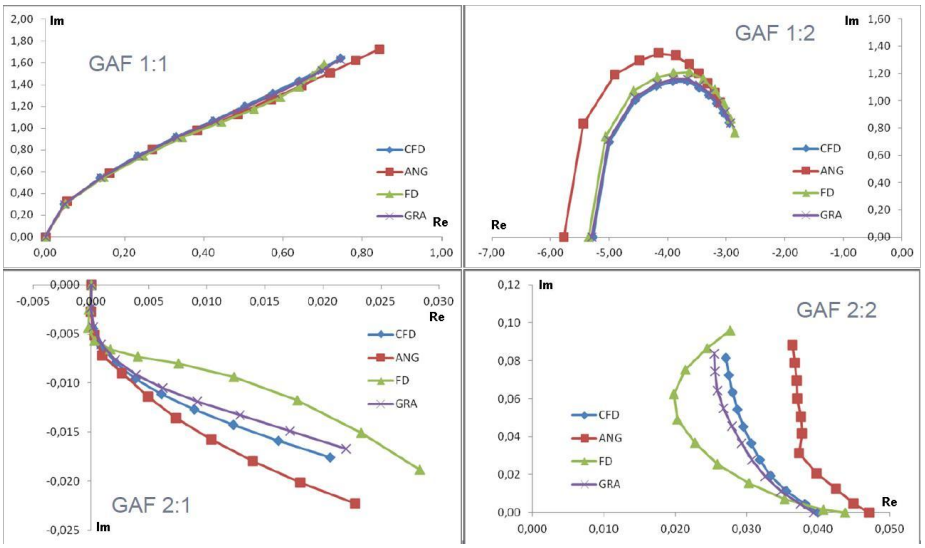

Figure 4: NACA64A010 generalized aerodynamic force evolution in function of k in the Real-Complex plane.

number chosen for the interpolation. All proposed methods are applied to adapt the POD basis to the new transonic Mach number, while maintaining the same angle of attack $\alpha = 0$ with the procedure described in Section 3. Finally, after having computed the interpolated basis, the method shown in Section 2.4, to calculate the Generalized Aerodynamic Forces, is applied. The obtained GAF are reported in Figure 4 and compared to their counterparts predicted using the linearization of the high-fidelity aeroelastic model at the same flight condition considered. Before analysing the results, a first consideration is made on the number of POD basis necessary to perform the interpolation. It should be noted that the finite difference interpolation method requires at least 3 POD basis to apply the interpolation procedure, unlike the Angle interpolation method that requires only 2 POD basis and the Grassmann interpolation method that require at least 2 POD basis. Also, the sensitivity analysis method presents a constraint in terms of POD basis choice for the interpolation, linked to the δ used for the calculation of the total derivative, as shown in Section 3.1. The other two methods do not present any constraints in terms of POD basis choice for the interpolation. In this paper, the Grassmann manifolds interpolation is applied using at least 3 POD basis because, as was shown in [7], the Subspace Angle and Grassmann manifold techniques in the case of one parameter variation give the same results if we use the same 2 POD basis for interpolation.

In Figure 4 the evaluated GAF are compared with the reference solution: the figure shows that only the Grassmann manifold interpolation method correctly tracks all the components of the reference GAF compared with the two other techniques that show a poor accuracy and instability in GAF reconstruction. In particular, we can see a shift of the GAF 1:2 using the angle interpolation method (red curve) and a tracking problem in GAF 2:1 and GAF 2:2 for the angle interpolation method and the sensitivity interpolation method. To better understand the difference between the GAF built by the different interpolation techniques a flutter boundary for the airfoil is proposed in Figure 5. The flutter behaviour shown in Figure 5 confirmed the results obtained by the GAF comparison. In particular, we can see a tracking problem for Mode 2 in terms of frequency by the model obtained by the subspace angle interpolation and sensitivity analysis method. Also a difference in the damping curve obtained by the finite difference method is visible.

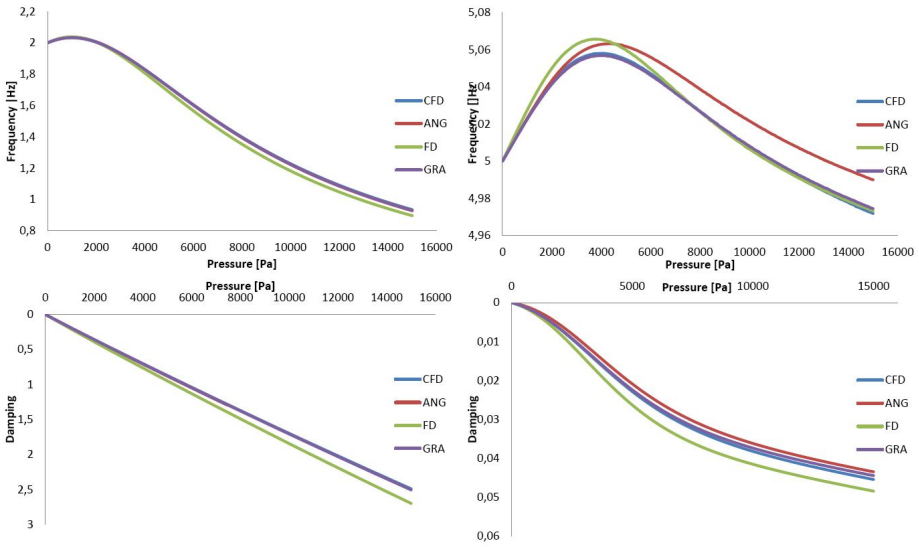

Figure 5: NACA64A010 flutter analysis comparisons.

Table 2: Set of precomputed ROM basis

Method	M_1	M_2	M_3	M_{Int}
Angle	0.725	0.75	X	0.738
Finite Diff.	0.7	0.725	0.75	0.738
Grassmann	0.7	0.725	0.75	0.738

A second example, in the same transonic environment, is performed but in this case the delta between the set of POD basis is reduced to 0.025 as shown in Table 2, still with a fixed angle of attack $\alpha = 0$. Table 2 also shows the new Mach number chosen for the interpolation.

In Figure 6 the evaluated GAF are compared with the reference solution: the figure shows that in this case, all the interpolation techniques give a better accuracy in the GAF reconstruction compared with the first case analysed.

We can see only a small shift of the GAF 1:2 built by the Subspace angle interpolation and a small deviation on GAF 2:2 built by the finite difference interpolation technique. To better understand the differences between the GAFs built by the different interpolation techniques, a flutter boundary for the airfoil is proposed in Figure 7. The flutter behaviour shown in Figure 7 confirms the results obtained by the GAF comparison. In particular, we can see better tracking for the three interpolation methods compared with the first case. From the analysis of these first two test cases, we can assert that the accuracy of the

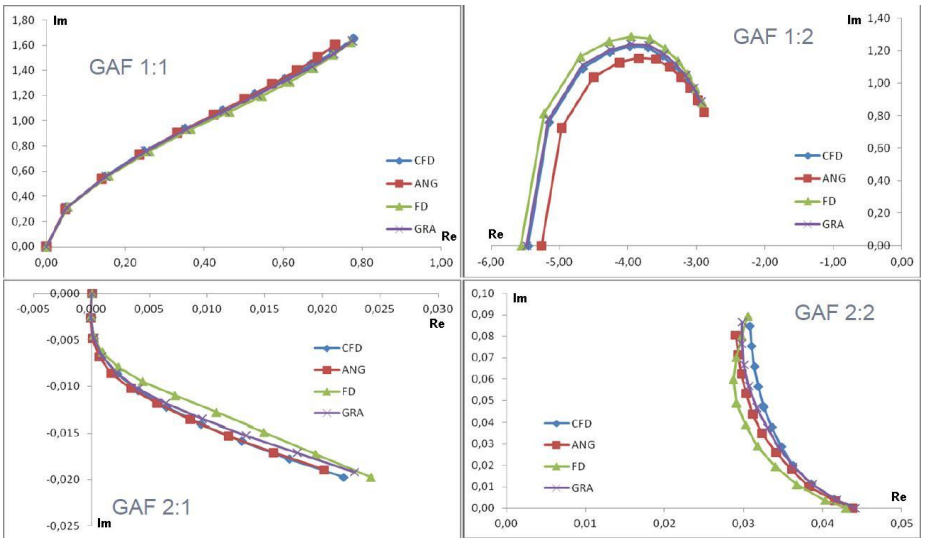

Figure 6: NACA64A010 generalized aerodynamic force evolution in function of k in the Real-Complex plane.

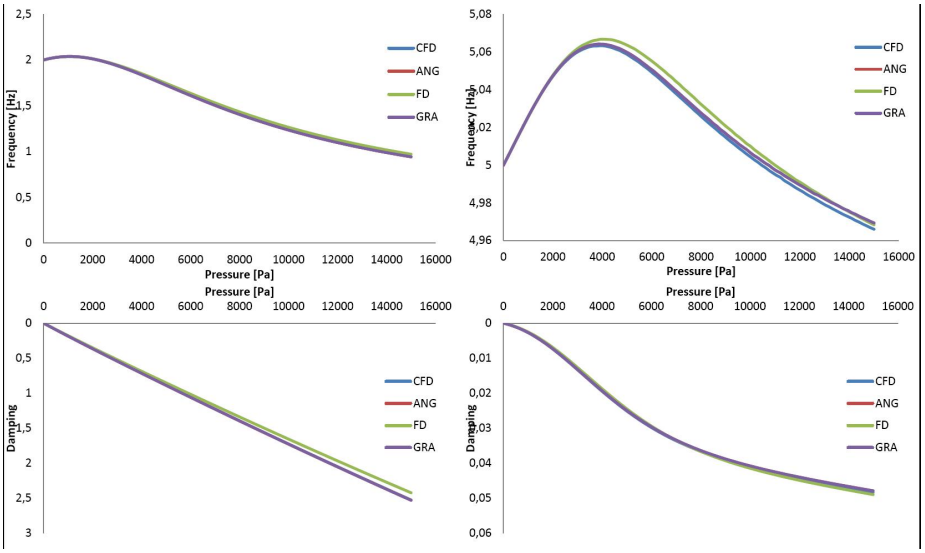

Figure 7: NACA64A010 flutter analysis comparisons.

Method	M_1	M_2	M_3	M_{Int}
Angle	0.8	0.8065	X	0.8033
Finite Diff.	0.8	0.8065	0.813	0.8033
Grassmann	0.8	0.8065	0.813	0.8033

Table 3: Set of precomputed ROM basis

results is inversely proportional to the delta between the precomputed POD basis. In particular, in the first test case, where the δ between POD basis in terms of Mach number was fixed at 0.5, the interpolation process contained the POD basis at Mach=0.8 that presented a shock compared with the other two that did not present a shock. In the second test case, where the δ between POD basis in terms of Mach number was fixed at 0.25, none of the POD basis considered for the interpolation process present a shock. Thus, if in the interpolation process, we consider a POD basis that presents a behaviour which is very different (presence of shock) regarding what we are trying to find (no shock), this could cause problems in terms of accuracy of the interpolated basis. In the next test case, a set of POD basis are precomputed in a high transonic range as shown in Table 3, but with a fixed angle of attack $\alpha = 0$. Table 3 shows that in this case the delta between the set of POD basis is reduced to 0.0065. In Figure 8 the evaluated GAF are compared with the reference solution: the figure shows that all the interpolation methods present some problems in GAF reconstruction. To better understand the difference between the GAF built by the different interpolation techniques, a flutter boundary for the airfoil is proposed in Figure 9. The flutter behaviour shown in Figure 9 confirmed the results obtained by GAF comparison, in particular we can see tracking problems for Modes 1 and 2 in terms of frequency and damping for the angle interpolation method and the finite difference method. Only the Grassmann manifold approach gave quite good results in terms of flutter prediction.

In this case we have investigated the capabilities of the different interpolation techniques in high transonic behaviour in the presence of shocks. In particular we have chosen a critical case when a small variation in terms of free stream Mach number causes a shock movement along the airfoil chord. Thus to obtain acceptable results in term of flutter prediction, the δ between POD basis in terms of Mach number is very small. After this first campaign of simulations we can affirm that in general the accuracy of the results is inversely proportional to the δ between the precomputed POD basis. Moreover, we can also assert that the more the flow condition approaches the transonic flight regime, the more the delta between precomputed ROMs is small.

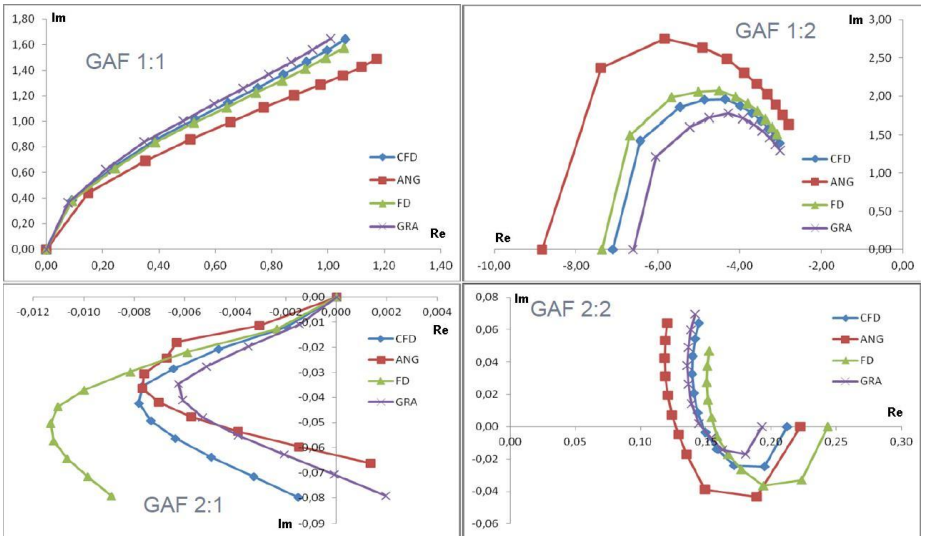

Figure 8: NACA64A010 generalized aerodynamic force evolution in function of k in the Real-Complex plane.

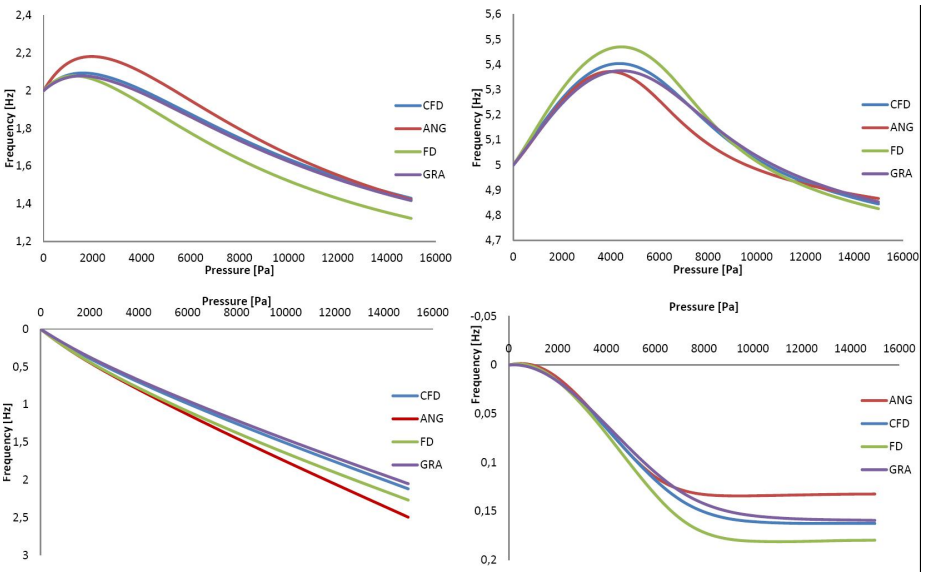

Figure 9: NACA64A010 flutter analysis comparisons.

In the next test we show the adaptation capability of the different methods selected to interpolate an aeroelastic system with simultaneous change in free-stream Mach number and angle of attack. The objective of this test is to show and compare the potential of the different interpolation techniques respect to a simultaneous change of parameters. At this point, as specified in Section 3, only the Grassmann interpolation method is able to take into account the simultaneous variation of parameters but, as shown in [10] in particular case it is possible to also use the other two methods. A set of three POD basis are pre-computed at different values of AoA and free-stream Mach number as shown in Table 4. Table 4 also shows the new AoA and Mach number values chosen for the interpolation.

In Figure 10 the evaluated GAFs are compared with the reference solution: the figure shows that only the Grassmann manifold interpolation method gives a good accuracy in GAF reconstruction compared with the other two techniques

Table 4: Set of precomputed ROM basis

Method	M_1	AoA_1	M_2	AoA_2	M_3	AoA_3	M_{Int}	AoA_{Int}
Angle	0.7	X	0.725	X	X	X	0.713	0.25°
Finite Diff.	0.7	X	0.725	X	0.75	X	0.713	0.25°
Grassmann	0.7	0.25°	0.725	0.25°	0.75	0.00°	0.713	0.25°

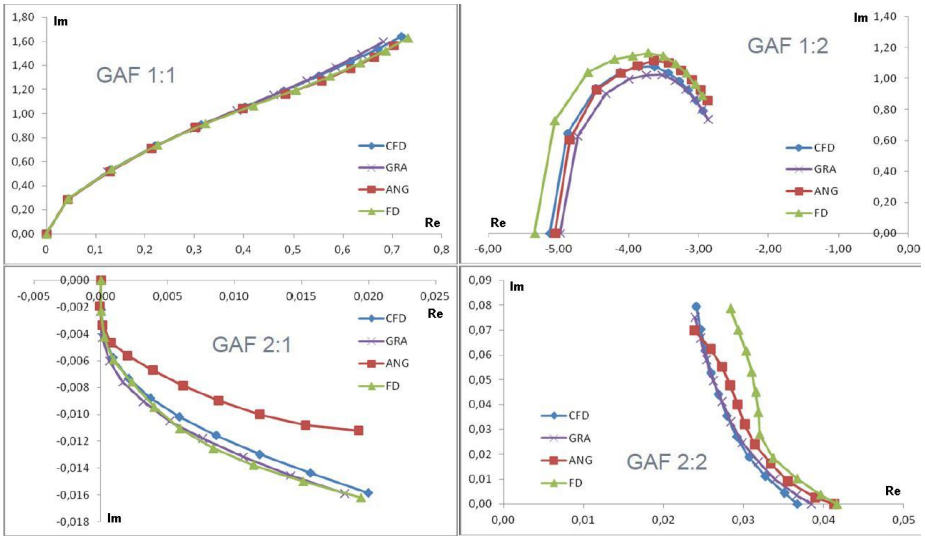

Figure 10: NACA64A010 generalized aerodynamic force evolution in function of k in the Real-Complex plane.

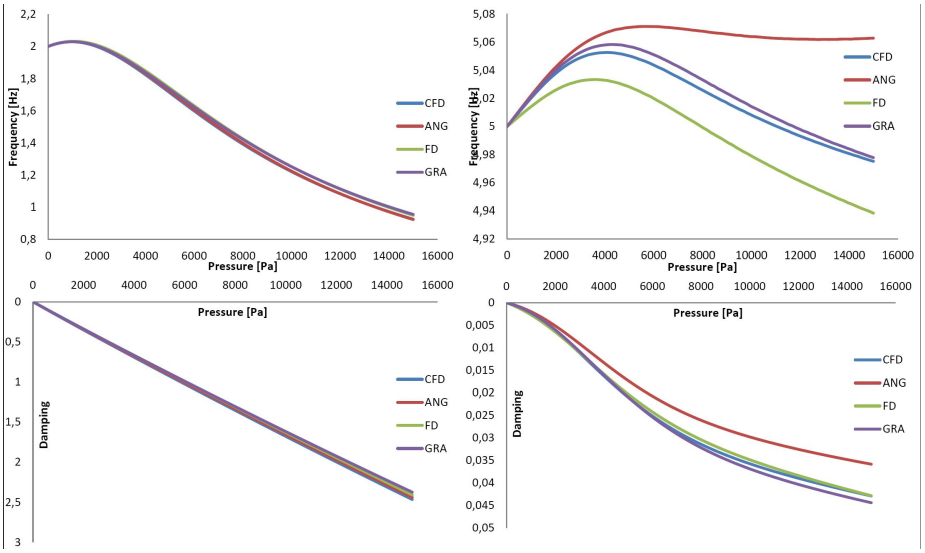

Figure 11: NACA64A010 flutter analysis comparisons.

that show some problems. To better understand the difference between the GAF build by the different interpolation techniques, a flutter boundary for the airfoil is proposed in Figure 11.

The flutter behaviour shown in Figure 11 confirmed the results obtained by the GAF comparison. In particular, we can see a tracking problem for mode 2 in terms of frequency for the angle interpolation method and finite difference method and also a tracking problem in terms of damping for the subspace angle interpolation approach. This test case confirmed that it is very difficult to obtain a good interpolated model with the angle interpolation method and the sensitivity analysis method when a simultaneous variation of multiple parameters (Mach and AoA) is taken into account. Generally is not possible to use the first two methods to consider the simultaneous variation of two parameters but, in some cases, it is possible if the variation in the AoA is not taken into account and only the variation in the Mach number is considered. However in this case we do not have any guarantees on the stability of the system obtained as shown in the example.

4.2 AMP Model

The next example is a representative Airbus commercial model that was tested in a transonic wind tunnel, also known as AMP model. See Figure 12(a). The

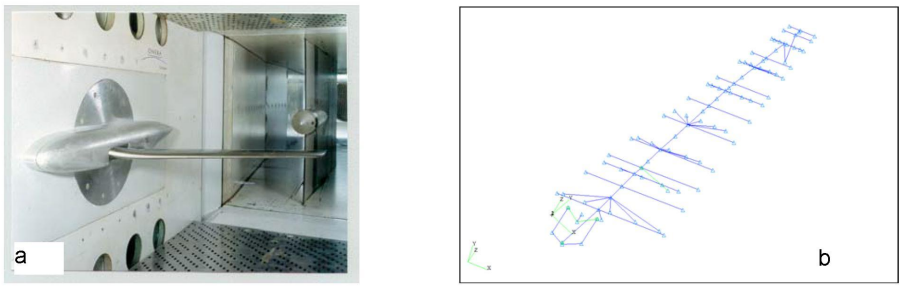

Figure 12: AMP model

Table 5: Set of precomputed ROM basis

	M_1	AoA_1	M_2	AoA_2	M_3	AoA_3	M_4	AoA_4
3 Points	0.78	0.79°	0.79	0.74°	0.82	0.61°	X	X
4 points	0.78	0.79°	0.79	0.74°	0.81	0.65°	0.82	0.61°

model was designed to exhibit bending-torsion flutter in the wind tunnel behaviour and for this reason only the first bending mode and the first torsional mode are take into account in the simulations. The aeroelastic full order computational model consists of a CFD structured Euler C-mesh with 576000 cells, which corresponds to 2880000 flow perturbation unknowns, and a condensed Finite Element structural model built by beam and concentrated mass. For more details see Figure 12(b). For all simulations total pressure and total temperature are fixed respectively at 90210 Pascal and 298 Kelvin. POD basis vectors are calculated using a frequency domain method of the snapshot approach. In order to compute the POD basis vectors in the transonic domain from Mach 0.78 to Mach 0.82, flow snapshots are evaluated at 13 non symmetrical spaced reduced frequencies between 0 and 0.225 for each structural mode for a total of 52 real POD vectors (2 Modes * 13 Frequencies * Real and Imaginary part of the snapshots). For all flight configurations a static coupling has been carried out to define the in flight shape of the model.

After computation of the snapshots, the POMs vectors are calculated and according to the energy criteria, 46 POD vectors are retained for the simulations. A set of four POD basis are precomputed at different trimmed flight conditions as shown in Table 5. The new trimmed flight conditions chosen for the interpolation are M_∞=0.8 and α_∞=0.7. The lift coefficient obtained for the reference model is 0.41. In this case, both the angle interpolation and sensitivity interpolation methods fail to generate a stable adapted ROM at the new trimmed flight condition. The reason behind this failure is due to the nonlinear variation of the POM vectors in the specified range of trimmed flight conditions. Two simulations with the Grassmann manifold interpolation method varying the number of the precomputed ROM basis are carried out, and then a stability study on the aeroelastic system is performed (theoretical details in Section 2.5).

In Figures 13-14 the evaluated unsteady pressure distribution for the first torsional mode at reduced frequency 0.225 on the upper surface (a, c) and on the lower surface (b,d) are compared with the reference solution. The figure shows a small local difference between the high order model and the interpolated model but in general we can confirm a good accuracy in the unsteady pressure reconstruction by the interpolation method.

Next, the stability analysis of the aeroelastic system is carried out for the full high order system, the system obtained by the classical POD approach, the system obtained by the interpolation method with three precomputed POD base and the system obtained by the interpolation method with four precomputed POD basis respectively. The results in terms of flutter pressure and its relative error compared to the reference, linearized high order model is shown in Table 6. In Figures 15-16 the flutter analysis for the case with four precomputed POD

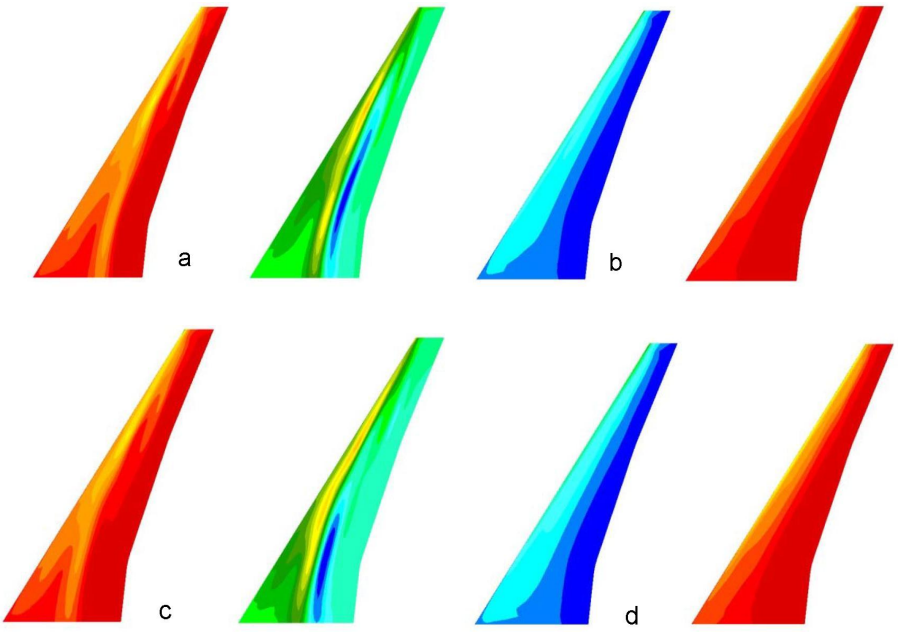

Figure 13: Real and Imaginary part of the unsteady pressure distribution on the wing surface for the first torsional mode at k=0.225 high order model.

Figure 14: Real and Imaginary part of the unsteady pressure distribution on the wing surface for the first torsional mode at k=0.225 interpolated model.

basis is compared with the flutter analysis obtained by the POD method and the reference high order solution. The figure shows that the flutter solution obtained by the interpolation method track well the solution obtained by the linearized higher order model.

Also a sensitivity analysis with respect to the choice of the origin point of the geodesic (Φ_0 of equation 44) for the Grassmann manifold interpolation is carried out and basically the results in terms of flutter prediction are nearly identical, which confirm the consideration shown in [7]. From the study of the results, we can assert that increasing the number of points for the interpolation, increase the accuracy of our interpolated model. This justifies in fact the idea of creating a database of ROM basis for the interpolation, as shown in [5].

4.2.1 Computational cost

An evaluation of the computational cost to build an aeroelastic POD based ROM of the AMP wing model for one fixed flight condition is shown in Table 7.

In Table 7 we have also shown the computational cost to obtain the same results with a high fidelity model and with the interpolation technique. From the analysis of these results, we can see that in the POD based ROM approach, as expected, the CPU time for generating the snapshots represents most of the computational cost. We can also see that the time for generating the snapshots and the high fidelity model is the same (same calculations). The CPU time to obtain the same results with an interpolated ROM is only 2 minutes. From this observation, we can see the importance and the potential of the technique of interpolation between POD basis.

	Flutter Pressure [Pa]	Error %
CFD	186868	Reference
POD	188393	0.82
Grass 3 points	174242	6.76
Grass 4 points	179292	4.05

Table 6: Flutter prediction and relative error.

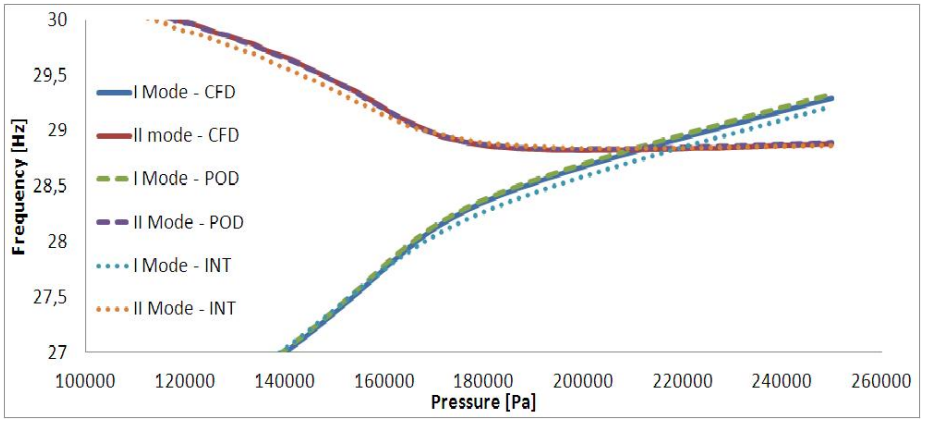

Figure 15: Figure 15: AMP model flutter analysis comparisons, frequency vs dynamic pressure

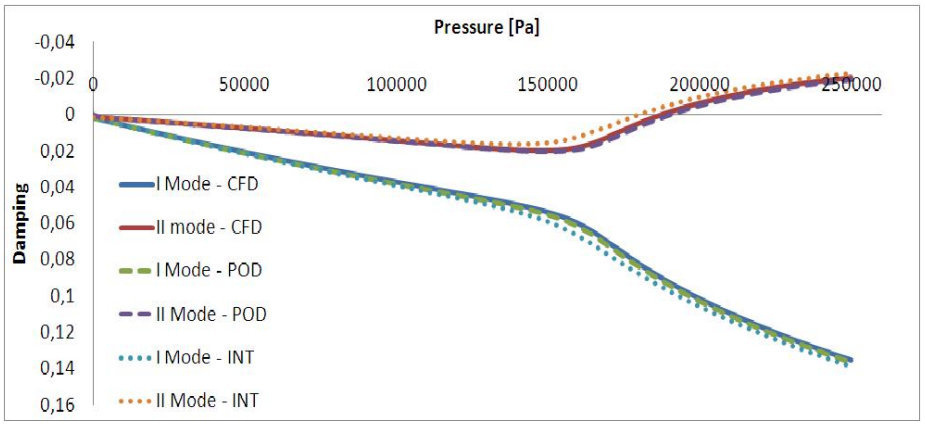

Figure 16: AMP model flutter analysis comparisons, damping vs dynamic pressure

Table 7: Computational cost 8 processor Linux cluster

	Computational cost
High Fidelity Model (26 CFD calculus)	5h
Snapshots generation	5h
POD/ROM Computation	4 min
Interpolated ROM computation	2 min

5. Concluding Remarks

Despite the accurate reproduction of the data from which it originates, the POD based reduced-order model lacks robustness away from the reference simulations. This is a serious limitation of the POD-based reduced-order models since most applications use reduced-order models in a predictive setting. The main objective of this paper is to present a complete set of tools that allows the interpolation between POD basis. Several procedures have been analyzed for the adaptation algorithm, in order to provide the highest degree of accuracy of the interpolated model. A critical review of the selected methods was presented, critically describing the advantages and drawbacks of the different approaches. Two aeroelastic systems were investigated: a NACA 64A010 wing section and a transonic wind tunnel model of a representative Airbus commercial aircraft. The adaptation capabilities of the different methods are compared in terms of GAF reconstruction in the first example and flutter analysis in the second example. The effectiveness of these approaches clearly depends on whether or not the POD modes exhibit a nearly linear dependence with respect to the variation of parameters. For this reason, it seems that the effectiveness of the methods is greatly reduced when approaching System non linearity zones.

6. Acknowledgements

This paper has been supported by "Direction des Programmes Aronautiques Civils" (DGAC/DTA/SDC)

References

[1] Hay A. Akhtar I., Borggaard J.T. On the sensitivity analysis of angle-of-attack in a model reduction setting. In *48th AIAA Aerospace Sciences Meeting including the New Horizons Forum and Aerospace Exposition*. Orlando - Florida, January 2010.

[2] Akhtar I. Borggaard J., Hay A. Shape sensitivity analysis in flow models using a finite difference approach. *Mathematical Problems in Engineering*, March 2010.

[3] Hay A. Borggaard J., Pelletier D. On the use of sensitivity analysis to improve reduced-order models. In *4th AIAA Flow control conference*. Seattle - Washington, June 2008.

[4] Amsallem D. Cortial J. Calberg K., Farhat C. A method for interpolating on manifolds structural dynamics reduced-order models. *International journal for numerical methods in engineering*, 2009.

[5] Amsallem D. Cortial J., Farhat C. Fast cfd-based aeroelastic prediction using a database of reduced-order models. In *International Forum of Aeroelasticity and Structural Dynamics*. Seattle - Washington, June 2009.

[6] Bui-Than T. Damodaran M., Willcox K. Proper orthogonal decomposition extensions for parametric applications in transonic aerodynamics. In *21th AIAA Applies Aerodynamics conference*. Orlando - Florida, June 2003.

[7] Amsallem D. Farhat C. An interpolation method for adapting reduced order models and application to aeroelasticity. *American Institute of Aeronautic and Astronautics*, 46(7):1803–1813, 2008.

[8] Amsallem D. Farhat C. Recent advances in reduced-order modelling and application to nonlinear computational aeroelasticity. In *46th AIAA Aerospace Sciences Meeting and Exhibit*. Reno - Nevada, January 2008.

[9] Lieu T. Farhat C. Aerodynamic parameter adaptation of cdf-based reduced-order models. In *45th AIAA Aerospace Sciences Meeting and Exhibit*. Reno - Nevada, January 2007.

[10] Lieu T. Farhat C., Lesoinne M. Pod-based aeroelastic analysis of a complete f-16 configuration: Rom adaptation and demonstration. In *46th AIAA/ASME/ACSE/AHS/ASC Structure, Structural Dynamics & Materials conference*. Austin - Nevada, April 2005.

[11] Mortchelewicz G.D. Flutter simulation using the linearized euler equations. In *39th Israel Annual Conference on Aerospace Sciences*. Tel Aviv - Haifa, February 1999.

[12] Mortchelewicz G.D. Application of proper orthogonal decomposition to linearized euler or reynolds-averaged navier-stokes equation. In *47th Israel Annual Conference on Aerospace Sciences*. Tel Aviv - Haifa, February 2007.

[13] Schmit R. Glauser M. Improvements in low dimensional tools for flow-structure interaction problems: Using global pod. In *42th AIAA Aerospace Sciences Meeting and Exhibit*. Reno - Nevada, January 2004.

[14] Bjork A. Golub G.H. Numerical methods for computing angle between linear subspaces. *Mathematics of Computation*, 27(127):579–594, July 1973.

[15] Thomas J.P. Hall K.C., Dowell E.H. Reduced-order aeroelastic modelling using proper-orthogonal decompositions. In *International Forum of Aeroelasticity and Structural Dynamics*. Williamsburg, June 1999.

[16] Willcox K. Unsteady flow sensing and estimation via the gappy proper orthogonal decomposition. *Computers & fluids*, 35(2):208–226, 2005.

[17] Absil P.A. Mahony R., Sepulchere R. Riemannian geometry of grassmann manifolds with a view on algorithmic computation. *Acta Applicandea Mathematicae*, 80(2):199–220, January 2004.

[18] De Boor C. Ron A. Computational aspects of polynomial interpolation in several variables. *Mathematics of Computation*, 58(198):705–727, April 1992.

[19] Beran P.S. Silva W.A. Reduced-order modelling: New approaches for computational physics. *Progress in Aerospace Sciences*, 40(1-2):51–117, February 2004.

[20] Begelfor E. Werman M. Affine invariance revisited. *Computer society conference on computer vision and pattern recognition*, 2:2087–2094, 1992.

[21] Gordon W.J. Wixom J.A. Shepards method of metric interpolation to bivariate and multivariate interpolation. *Mathematics of Computation*, 32(141):253–264, January 1978.